Fabricating Arrays of Single Protein Molecules on Glass Using Microcontact Printing

J. P. Renault,[†,‡] A. Bernard,[§,||] A. Bietsch,[§] B. Michel,[§] H. R. Bosshard,[†] and E. Delamarche*[,§]

IBM Research, Zurich Research Laboratory, CH-8803 Rüschlikon, Switzerland, and Department of Biochemistry, University of Zurich, Winterthurerstr. 190, CH-8057 Zurich, Switzerland

M. Kreiter,[⊥] B. Hecht,*[,#] and U. P. Wild

Physical Chemistry Laboratory, Swiss Federal Institute of Technology (ETH), 8092 Zurich, Switzerland

Received: June 20, 2002; In Final Form: October 14, 2002

Microcontact printing biomolecules from elastomeric micropatterned stamps onto surfaces is a versatile method to prepare surfaces for diagnostic applications. We show how to create patterns of proteins having a lengthscale lower than 100 nm using high-resolution microcontact printing. The elastomeric stamps used have meshes composed of 100- and 40-nm-wide lines, arrays of 100 × 400 nm^2 features, and arrays of 100-nm-wide posts. The spherical geometry of the posts on the stamps contributes to reduce the printed areas below the effective size of the molded features. Proteins adsorb onto the hydrophobic surface of the stamp during the inking step, and by varying the concentration of the protein solutions, it is possible to adsorb a single or a few protein molecules, such as antibodies (fluorescently labeled) or green fluorescence proteins, on each of the elements forming the high-resolution pattern of the stamp. The transfer of the proteins from the stamp to a hydrophilic glass surface occurs during the printing step. Characterization of the printed patterns using atomic force microscopy and fluorescence confocal microscopy reveals sites unoccupied or occupied by one or more protein molecules that are located within 50 nm of the expected printed locations. The placement of a small number of protein molecules on a surface at precise locations is the key to localizing and identifying single proteins and might constitute a method of choice to study single protein molecules on surfaces.

Introduction

The development of molecular machines[1−3] and, more specifically, the development of artificial architectures that comprise biological objects requires positioning and connecting of molecular components with high specificity and precision.[4,5] One possible approach toward this end is to direct the synthesis of the building blocks where needed by using self-assembly principles.[6,7] Assembling predefined objects at desired locations, in parallel or one after each other, constitutes an alternative strategy of assembly.[8,9] Both methods can be combined by using template-directed self-assembly. This area of research has experienced considerable progress, in part owing to the development of nanotechnologies and in part because studying the variations in the properties of single molecules should not be plagued by averaging artifacts. This might be particularly true in the case of proteins: Proteins can play the role of specific ligands, receptors, or units in electrochemical pathways, can serve as adhesive or cohesive molecules, or act as catalysts or chemo-mechanical elements. In addition, direct observation of the mechanical properties of proteins, for example, is invaluable in validating the hypothesis obtained from structural determinations.[10−13] Investigating the binding between one antibody and one antigen on a surface[14] is a specific example that necessitates manipulating single protein molecules and that can give important insights into the mechanism and strength, kinetic, and thermodynamic characteristics of the association event, and maybe on heterogeneous immunoassays in general.[15−17]

We pioneered the direct patterning of proteins onto surfaces using microcontact printing (μCP)[18] and now extend this method to the fabrication of arrays of single protein molecules on surfaces. The direct[18−25] or indirect[26−31] patterning of proteins using μCP relies on using a microstructured elastomer (a stamp). The patterning of surfaces using micropatterned stamps was originally developed by Whitesides et al. for self-assembling alkanethiols on Au with spatial control.[32,33] Stamps are made from poly(dimethylsiloxane) (PDMS) by curing liquid prepolymers of PDMS on a lithographically prepared master. Masters are usually Si wafers covered with a patterned photoresist or, for preparing higher resolution masters, Si wafers with a patterned electron-beam (e-beam) resist.[34,35] The pattern in the resist can be transferred into the Si substrate by deep reactive ion etching to yield more robust and reusable masters. μCP is a versatile technique because low-resolution stamps (stamps with features of a few micrometers) are simple to fabricate and can be used with a variety of inks and substrates.[33,36] Improving the mechanical properties of the PDMS elastomer used to replicate masters and using inks having small diffusion characteristics were keys to microcontact print patterns having sub-100 nm resolution.[34] In previous work, alkanethiols that have a molecular crossection of 0.2 nm^2 were utilized, and two hundred of them were needed to cover the width of a 100-nm-wide line.

In this paper, we show how to microcontact print single protein molecules such as antibodies (whole immunoglobulins G) and green fluorescent proteins[37] (GFPs) onto a glass surface

* To whom correspondence should be addressed. E.D. (emd@zurich.ibm.com) or B.H. (bert.hecht@unibas.ch).

† University of Zurich.

‡ Current address: Laboratoire de Radiolyse, CEA/Saclay, F-91191 Gif sur Yvette, France.

§ IBM Research.

|| Current address: Indigon GmbH, Albrechtstrasse 9, 72072 Tübingen, Germany.

⊥ Current address: Max Planck Institut für Polymerforschung, Ackermannweg 10, 55128 Mainz, Germany.

Current address: Nano-Optics Group, Institute of Physics, University of Basel, Klingelbergstrasse 82, CH-4056 Basel, Switzerland.

10.1021/jp0263424 CCC: $25.00
Published on Web 12/10/2002

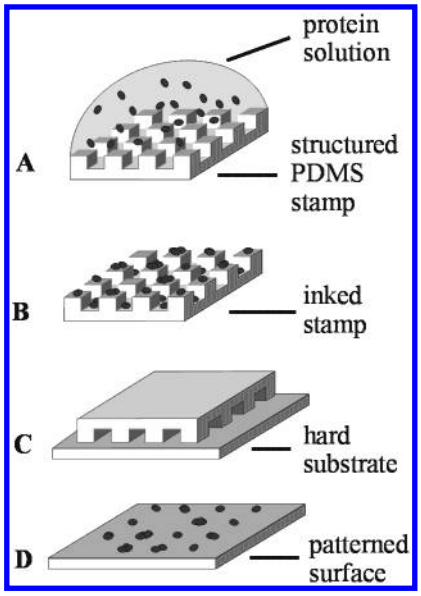

Figure 1. Fabricating high-resolution patterns of proteins using μCP starts with (A) and (B) depositing proteins from solution onto the surface of a stamp during an inking step and (C) transferring the proteins to a substrate in the area of contact to (D) yield a patterned substrate once the stamp has been removed.

by decreasing the printed zones of structures on a PDMS stamp below 100 nm and by diluting the molecules in the ink, Figure 1. We then employ atomic force microscopy (AFM) and fluorescence scanning confocal microscopy to characterize the printed patterns of proteins. Preparing regular patterns over large scales (200−400 μm with more than 10^5 dots for example) allows the observation of a large number of protein molecules at known locations. Confocal fluorescence microscopy benefits from the placement of molecules as arrays onto untreated glass and can consequently be used to count the number of proteins transferred per feature down to the single-molecule level.

Experimental Section

Preparation of High-Resolution Stamps. High-resolution masters (molds) for stamps used for printing the smallest features were fabricated by exposing electron-beam-sensitive photoresists spin-coated on 4″ silicon wafers with e-beam lithography (XLITH, GmbH, Illerieden, Germany). The developed resist acted as a mask for selectively etching the Si substrate using a reactive-ion etcher (STS, Bristol, U.K.). The resist was removed after this etch step using an oxidizing plasma, and a fluorinated layer (∼5-nm thick) was finally deposited from plasma onto the patterned Si mold. Dry etching of the masters was performed with special attention to create small features with slanted sidewalls and size-dependent etching to reduce the etch depth of smaller features compared to larger features. Large features with etch depths of 60, 120, and 240 nm were tested. The stamps corresponding to the masters with the 120-nm-deep large features gave the best results: they had 100-nm-wide posts that were 60 nm high and 80-nm wide posts that were shorter than 50 nm thus keeping the maximal aspect ratio <1. The reactive-ion-etching recipe had a slow etching rate at the bottom corners of the posts, which produced rounded caps for small dots or lines and posts with semispherical tops.

Liquid prepolymers of a PDMS material, referenced in the text as material B,[35,38] were carefully mixed by hand and placed on the Si molds. Curing of the PDMS polymer was done at 100 °C for 3 h. The lithographic layout of the stamps included a series of 400 × 400 μm^2 fields of various high-resolution structures: Arrays of posts, ridges, and linelet features and mesh structures with critical dimensions lying between 40 and 600 nm. The overall areal fill factor averaged over small and large features was 12.5%. Areal fill factors of meshes and arrays of dots were typically lower and depended on the printing force. Because the lithographic layout of the stamps included 400 × 400 μm^2 areas (filled with various high-resolution structures) that were surrounded by a 800-μm wide area containing support structures, stamps were stable enough against pressure-induced collapse to allow printing by hand.[38−40] The stamps were handled manually using tweezers and were lightly pressed, using the tips of the tweezers, to initiate and help the contact of the stamp with the substrate propagate during printing.

Inking of Stamps and Microcontact Printing. FITC fluorescently labelled IgGs from rabbit, BSA, and avidin were purchased from Sigma and GFP from Clontech. The rabbit IgGs had 4−5 fluorescein-isothiocyanate labels per molecule on average and were received dissolved at a concentration of ∼5 mg mL^{-1} in PBS (phosphate-buffered saline, pH 7.4, Sigma). All biomolecules were stored at 4 °C in the dark, and their diluted solutions in PBS were prepared shortly before inking and printing experiments to minimize denaturation of the proteins.

Typically, proteins were deposited on the stamps by covering these with ∼20 μL of a 5 μg mL^{-1} solution of protein in PBS for 45 min. The stamps were placed in a polystyrene Petri dish containing droplets of water to prevent the evaporation of the ink solution during inking. Successful printing of GFPs required inking stamps with a solution of GFP having a concentration >50 μg mL^{-1}. The stamps were rinsed with PBS (3 × 10 mL) and deionized water (3 × 10 mL) and then immersed in a large volume (1 L) of deionized water before being dried under a stream of N_2, to prevent precipitation of residual salts or proteins. Inked stamps were positioned by hand over glass substrates (microscope slides from Menzel-Gläser, Germany) and brought into contact with the substrate for 1 s before being removed by hand. All printing experiments were followed under a far-field optical microscope (from Nikon) in order to control that no collapse of the pattern of the stamps onto the substrate occurred over large areas. Some stamps could be used about 50 times without degradation of their printing capability when cleaned by sonication in a water:ethanol mixture (80:20) for 5 min after each inking and printing cycle. The results reported here were obtained using stamps for only one inking and printing experiment.

Visualization of the Printed Patterns of Proteins. AFM pictures were recorded using a Nanoscope Dimension 3000 (Digital Instruments, Santa Barbara, CA) operated in tapping mode using SuperSharpSilicon tips (Nanosensors, Norderfriedrichskoog, Germany) having a tip radius <5 nm (guaranteed by the manufacturer). All images for measuring the dimensions of patterns were taken with the same tip and using a 2 × 2 μm^2 or a 20 × 20 μm^2 area. The same pattern was recorded at the beginning and at the end of each series of experiments to verify that no change in resolution had occurred during the experiments.

Samples microcontact printed with fluorescently labeled proteins were investigated using a home-built sample scanning fluorescence confocal optical microscope.[41] One of the two lines of an argon ion laser (514.5/488 nm) was used to excite the fluorescence. The light was coupled into a single mode fiber, the exit of which served as the excitation pinhole and emits a perfect Gaussian beam. The light emitted by the end of the fiber was attenuated to a few μW so as not to saturate the optical

transitions of the chromophores. The beam was then collimated and directed via a dichroic mirror onto the entrance pupil of an oil immersion objective (Leica, 1.3 NA, ×60), which focused the beam to a diffraction-limited spot (~250 nm) onto the surface of the glass substrate. The fluorescence from the sample was collected by the same objective and directed through the dichroic mirror to an avalanche photodiode (EG&G, SPCM-AQR, Canada). A holographic notch filter for the respective excitation wavelength removed the remaining Rayleigh-scattered light. Images were recorded by scanning the sample through the laser focus and recording the number of collected photons at each pixel. Typical integration times per pixel ranged from 1 to 10 ms. Alternatively, the sample position was fixed, and the number of detected photons per time interval was measured continuously to create a time trace. Note that the sample piezoelectric scanner was actively linearized over the full 60 × 60 μm^2 scan range with an absolute accuracy of better than 10 nm. The overall detection efficiency of the setup was ~6.5%. Such a high detection efficiency is instrumental when detection of single chromophores is desired. Similar studies are in principle possible with commercial microscopes; however, the detection efficiency should then be evaluated carefully.

Results

High-Resolution Microcontact Printing of Proteins. A major challenge for the microcontact printing of very small dots and lines is the reduction in stability of elastomeric features of shrinking dimension. The mechanical stability of tall cylindrical pillars, for example, diminishes when the pillars are made smaller rendering them more prone to collapse during inking and printing. Successful printing of small and large patterns at the same time requires a minimal height of the features, however. High-resolution stamps fabricated on silicon-on-insulator wafers[38] with vertical sidewalls and planar tops were tested with different feature heights of 60 and 120 nm, but these stamps proved inefficient to print very small patterns and single protein molecules because of the limited mechanical stability of their high-aspect-ratio posts. Other routes to create stamps with more stable (less deep) high-resolution features were not effective or unpractical for this work. Instead, we preferred to reduce the areas of contact between the stamps and substrates by molding posts that had a semispherical top. Most advantageous was to have the smaller posts with less height, the larger features with proportionally larger height, and tall support structures surrounding zones with small patterns to remove part of the printing pressure from the high-resolution areas.

We prepared and characterized masters and stamps with dots, lines, and meshes having feature sizes from 40 nm up to 600 nm to test high-resolution printing. A single type of high-resolution structure was repeated inside 400-μm-large fields that were surrounded by micrometer-sized support meshes. Some of the patterns that were used in the current work are short lines (linelets) 400 nm long, 100 nm wide, and spaced with a 800-nm pitch, 80-nm dots spaced in a square lattice with a pitch of 320 nm, and 100-nm dots spaced in a square lattice with a pitch of 400 nm, Figure 2. Patterns were made with variable heights; the 100-nm-wide posts were 60 nm high as shown in the three-dimensional AFM image in Figure 2, and the posts are close to spherical with a diameter of 120−140 nm and a height of 60 nm. Estimation of the contact area between the posts and a glass surface during printing were calculated with (JKR model) and without (Hertz model) adhesion forces between the stamp and the substrate. These calculations suggested that such posts have an area of contact with a diameter between 20 and 110 nm when

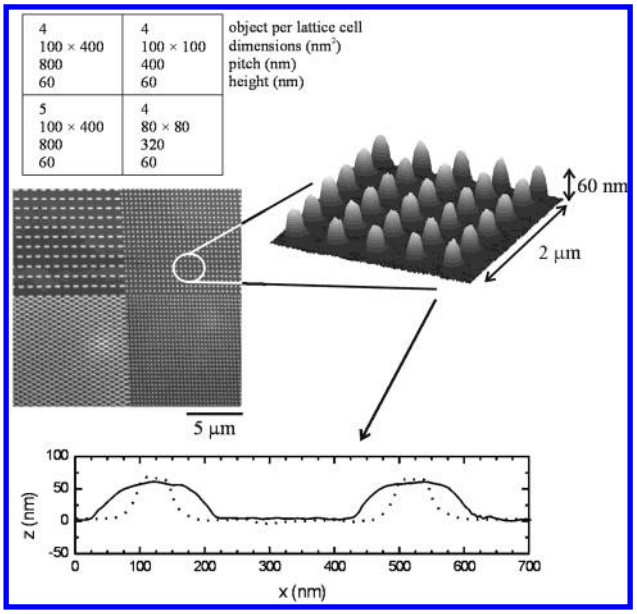

Figure 2. AFM images obtained on a PDMS stamp molded from Si master that was prepared using e-beam lithography and reactive ion etching. The patterns in this Figure consist of linelets (short lines) with a 400-nm-length and a 100-nm-width spaced on a square lattice with a 800-nm-pitch (top left quadrant). The next quadrant (bottom left) comprises a similar pattern but with one more linelet in the center of the lattice cell. 80-nm posts spaced with a pitch of 320 nm (bottom right) and 100-nm posts spaced with 400 nm (top right) populate the last two high-resolution quadrants. The 100-nm posts, used throughout this work, are 60 nm tall as is visible in the three-dimensional AFM representation. The AFM scans of these posts on the stamp (solid line) and of their counterparts on the master (dotted lines) are convolved with the geometry of the AFM tip, which reduces the width of the features in the master and broadens the posts on the stamp. The scan corresponding to the master has been inverted for clarity.

exposed to a printing pressure of 10 g per cm^2. These posts are 60 nm shorter than adjacent larger features, and it is likely that some water condensates spontaneously when these posts come into close contact with the hydrophilic substrate. For these reasons, the pressure exerted onto these posts during printing may decrease, which should result in smaller effective areas of contact.[38,42,43] These posts that are used throughout this work are referred to as 100-nm posts because they result from 100-nm-wide exposures in the e-beam lithography writer. Developing the exposed resist, reactive ion etching the Si mold, and surface tension phenomena occurring when the polymer is released from the mold all contribute to the final geometry of the patterns. The resulting posts have a 140-nm base and a top diameter <50 nm, Figure 2. Typically, the smaller 80-nm posts did not provide reproducible printing experiments probably because their height (<50 nm) rendered them insufficiently mechanically stable. Examples of other structures used in Figure 3 are 40-nm-wide ridges spaced in an 800-nm mesh and 100-nm-wide ridges spaced in a 2-μm mesh.

We use mainly antibodies in solution as the ink to build on previous work as much as possible and to investigate the rules for microcontact printing down to the single molecule level.[18,21] Inking the stamps is simple. High-resolution stamps made of material "B"[35] are hydrophobic (advancing and receding contact angles with water of $\Theta_{adv} \sim 115°$ and $\Theta_{rec} \sim 95°$, respectively) and have a surface chemistry comparable to those made of Sylgard 184, and both kinds of stamps have the same tendency to adsorb proteins from a solution. It takes typically less than an hour to form a complete layer of antibodies on the stamp by adsorption from a PBS solution with a concentration of

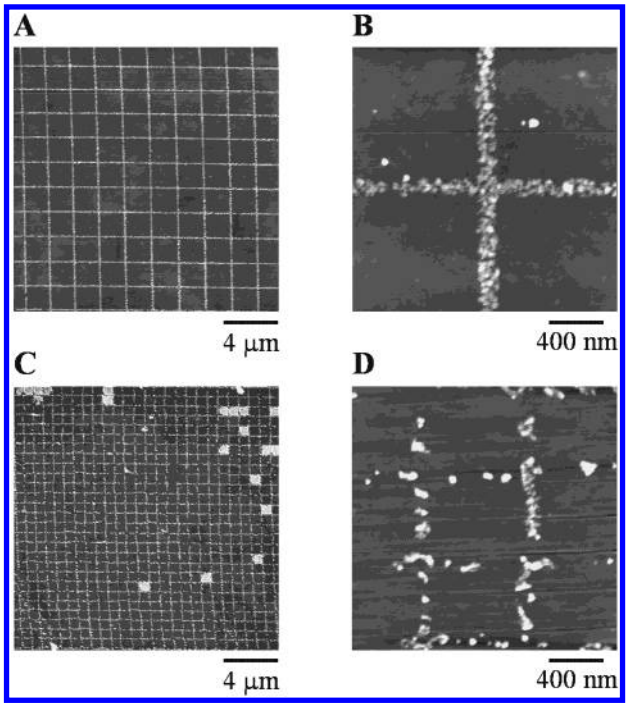

Figure 3. AFM images of antibodies microcontact printed on glass using high-resolution PDMS stamps. The patterns in (A) and (B) were produced using a grid of 100-nm-wide lines that were separated by 2 μm, and the patterns in (C) and (D) used 40-nm-wide lines separated by 800 nm. Stamps were inked for 45 min with a 5 μg mL^{-1} solution of rabbit antibodies in PBS for all experiments.

antibodies ≥ 5 μg mL^{-1}.[18] The AFM images in Figure 3, parts A and B, show antibodies printed onto glass using patterns formed by 100-nm-wide ridges arranged in a mesh having a 2-μm pitch. It is obvious from the figure that high-resolution μCP is not restricted to the patterning of small areas only but that patterns can extend over hundreds of micrometers. The patterns of proteins in Figure 3A reveal that inking of the stamp, printing, and transferring the proteins occurred in a homogeneous manner.

Figure 3B shows high-quality lines of printed proteins having a texture in which single elements are discernible. This represents the narrowest pattern that we could use successfully to print high-resolution patterns of proteins (see below). The proximity of the objects detected by the AFM in Figure 3B points to the dense deposition of the antibodies onto the stamp during inking. Antibodies (in solution) are described as disks 10 to 14 nm in diameter and a few nanometers thick.[17,44−46] We expect to have a maximum of maybe seven antibody molecules across the lines forming the patterns. Therefore, the characteristics of these patterns should be proportionally more affected by the exact position and shape of its constituents here than when patterns are much larger.[19,21,47] The experiments shown in Figure 3, parts C and D, in which 40-nm-wide lines constituted the mesh reveal that using narrower lines did not increase the lateral resolution of the printed patterns of antibodies. We do not think that mechanical instabilities of these patterns of the stamp account for the "defects" observed in the image.[38,40] Possibly, the transfer of proteins initiated in the regions of contact and propagated to some of the recessed regions of the stamp because of the lateral interactions between the protein layer covering the stamp.[48] The inking and printing conditions were identical for all four images of the figure, but the patterns printed with the smaller mesh comprise irregular aggregates of proteins that are dispersed on a width of ~100 nm. The average thickness of the proteins on the surface is 4−5 nm and is consistent with earlier work.[18]

We tried to reproduce these high-resolution printed patterns with proteins of various molecular weights, GFP (30 kDa), bovine serum albumine (BSA, 66 kDa), and avidin (66 kDa). The characteristics of the printed patterns using avidin and BSA were very similar to their counterparts made using antibodies, whereas GFP has to be more concentrated in the ink solution (up to 500 μg mL^{-1} in PBS) to obtain dense patterns of proteins such as the one in Figure 3B. This observation is consistent with previous observations, i.e., that small proteins interact less with uncharged surfaces than do large proteins.[49,50]

Using arrays of posts, we could isolate some of the antibody aggregates observed in the previous experiments using the meshes. Isolated features such as dots are less stable than grids formed with lines of similar width however, and we could not print arrays of dots smaller than 100 nm in a well reproducible manner. We were consequently limited to printing antibodies using the 100-nm posts, Figure 4. This pattern was optimal in terms of such a stability and separation among the printed features. Aggregates in Figure 4A are regularly spaced on the substrate, occupying 70% of the potential printing sites, and are within 50 nm of the positions defined by the lithographic pattern. Despite this variation in position and the existence of empty spots, the pattern is clearly visible even on a smaller scale, Figure 4B. The positions of the printed proteins relative to the lithographic pattern are likely to originate from the distribution of the proteins inked onto the posts. Proteins deposited from solution near the periphery of a 100-nm-wide post will at most be printed 50 nm away from the center of the pattern.

The statistical distribution of the size of the aggregates is reported in Figure 4C. Analysis of these data and data from a large number of images for this and for other samples prepared similarly suggests the existence of five distinct populations that have each a size below 2000 nm^2, discernible in the graph of Figure 4C. The smallest objects are ~350 nm^2 in size, and the larger objects in the graph can apparently be classified in populations having an area of $n \times 350$ nm^2. The lateral size of a protein molecule observed with an AFM depends on the conformation and orientation of the protein on the surface to some extent and on the scanning conditions (e.g., geometry of the AFM cantilever, force applied, ambient medium, etc.). A size of 350 nm^2 is plausible for a single antibody molecule imaged on a surface by a tip having a radius <5 nm.[17,44] We suggest that the aggregates consist of one to five antibodies, and we infer from the histogram in Figure 4C that ~30% of the occupied sites may correspond to a single antibody molecule. To obtain a second, independent characterization of high-resolution patterns of printed proteins we performed confocal fluorescence microscopy experiments.

Analysis of the Patterns using Confocal Fluorescence Microscopy. Very few techniques can detect and characterize single molecules on surfaces. Although confocal fluorescence microscopy does not have the spatial resolution of AFM, it can detect individual fluorophores on a surface with submicrometer resolution.[51] We made high-resolution arrays of proteins on glass using the method described above, first using fluorescently labeled antibodies and second using GFPs. The confocal fluorescence images obtained for microcontact-printed fluorescein-tagged antibodies are shown in Figure 5. The first type of pattern consists of arrays of linelets spaced with a 800-nm pitch, Figure 5A. The dimension of this pattern is large enough to be optically resolved. The distribution of intensities seems wide, and most

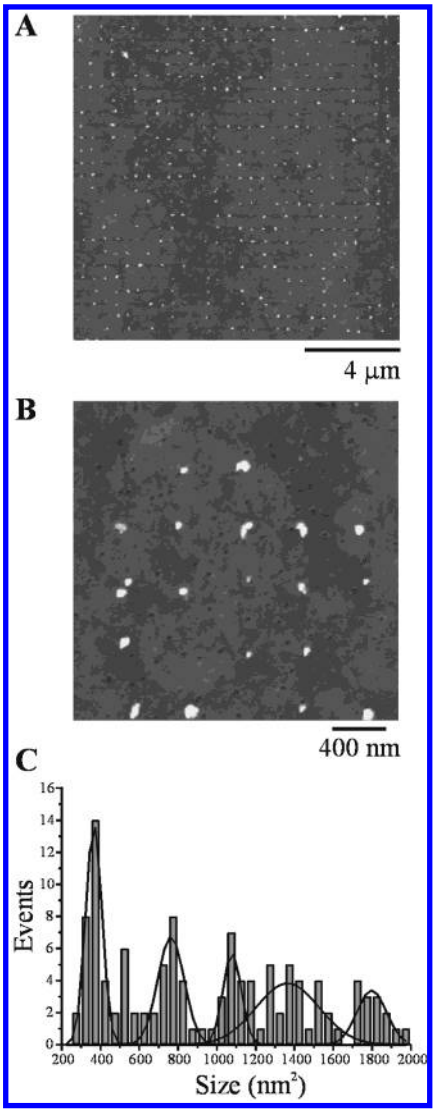

Figure 4. High-resolution patterns of antibody molecules microcontact printed on glass as characterized using an AFM. (A) This pattern was formed by printing rabbit antibodies using 100-nm posts on a PDMS stamp inked with a 5 μg mL^{-1} solution of protein in PBS for 45 min. (B) This higher resolution image reveals that the printed areas comprise none, one, or only a few protein molecules forming aggregates. (C) The size distribution of the aggregates suggests that they contain a discrete number of ~350-nm^2 proteins. The line indicates the Gaussian fit used to estimate the size distributions.

of the sites exhibit fluorescence. The image in Figure 5B corresponds to antibodies printed from the 100-nm posts. This time, no fluorescence is detected in one-third of the lattice points, and many dots exhibit a similarly low or medium fluorescence. Schmidt et al. demonstrated that it is possible to extract the number of chromophores in a cluster by measuring the fluorescence intensity emitted by the cluster.[52] The fluorescence intensity of a cluster is determined by fitting a Gaussian to its fluorescent peak. The volume of the Gaussian then corresponds to the fluorescence intensity. Here, we analyze the fluorescence images in a similar way. However, we take advantage of the deterministic placement of the fluorescently tagged antibodies in a regular grid provided by the high-resolution μCP process. The data analysis procedure is as follows: in a first step, the measured pattern is described analytically as a lattice defined by the base vectors $\mathbf{a}_1$ and $\mathbf{a}_2$ and an offset $\mathbf{x}_0$

$$\mathbf{x}_k = \mathbf{x}_0 + i(k)\mathbf{a}_1 + j(k)\mathbf{a}_2 \quad (1)$$

where k is an integer used to label all lattice points $\mathbf{x}_k$ inside of an image, $i(k)$ and $j(k)$ being the integer coefficients. The best values for $\mathbf{a}_1$, $\mathbf{a}_2$, and $\mathbf{x}_0$ yield a maximum intensity averaged over all lattice points within the image, thus providing a well-defined criterion for the determination of the lattice parameters. In the following, we assume that the observed pattern can be described as an array of two-dimensional Gaussian intensity profiles. The centers of these profiles, given by the vector r_k, may vary within the area of the dots.

$$I(x) = I_0 + \sum_{k=1}^{N} I_k \frac{1}{2\pi\sigma_{x,k}\sigma_{y,k}} \exp\left(-\frac{1}{2}\left(\left(\frac{x-x_k}{\sigma_{x,k}}\right)^2 + \left(\frac{y-y_k}{\sigma_{y,k}}\right)^2\right)\right) \quad (2)$$

where x_k and y_k are the Cartesian components of $\mathbf{r}_k$ and $\sigma_{x,k}$ and $\sigma_{y,k}$ are the widths of the kth spot in two dimensions. The fit of eq 2 to the measured intensity distribution is performed iteratively. One iteration consists of fitting each spot individually as a two-dimensional Gaussian using the Levenberg−Marquard algorithm. The fit is performed to minimize the difference between the measured data and a distribution, calculated according to eq 2, without the contribution of the spot to fit. Randomizing the order in which the spots are analyzed leads to a better convergence. Finally, this fit yields integrated intensities of the kth spot I_k with a standard deviation σ_{I_k}.

The best guess for the probability of a certain intensity per dot, $P(I)$, is then obtained by calculating a convolution of the intensities as obtained from the fit with the corresponding standard deviations

$$P(I) = \frac{1}{N}\sum_{k}^{N} \frac{1}{\sigma_{I_k}\sqrt{2\pi}} \exp\left(-\frac{1}{2}\left(\frac{I-I_k}{\sigma_{I_k}}\right)^2\right) \quad (3)$$

The intensity distribution obtained for Figure 5A shows several distinct maxima of intensity, which is expected from the relatively large area of the printed features (100 × 400 nm^2) and the likelihood that they comprise several fluorescent centers (several printed antibody molecules each conjugated with four to five fluorophores). The small, narrow peak at $I = 8$ of the graph in Figure 5C is assigned to the sites of the lattice without any protein, and most of the lattice points are occupied by three or more proteins. A similar analysis of the pattern comprising the smaller printed areas, Figure 5B, reveals less distinct maxima of intensity, corresponding to zones with zero ($I = 3$), one ($I = 8$), or two protein molecules ($I = 13$), see Figure 5D. The dots without fluorescent centers yield a positive intensity maximum due to an overall background signal. It should be noted that the addition of the appropriate background signal in the fitting routine leads to instabilities in the fitting routine. The total intensity distribution can be regarded as a sum of Gaussian functions $G_n(I)$, where n denotes the number of protein molecules per lattice point:

$$P(I) = \sum_{n} P_n G_n(I) \quad (4)$$

and

$$G_n(I) = \frac{1}{\sqrt{2\pi}\sigma_{I_n}} \exp\left(-\frac{(I-I_n)^2}{2\sigma_{I_n}^2}\right) \quad (5)$$

where P_n is the integrated probability for finding n proteins at one spot. If it is assumed that there is no interaction between

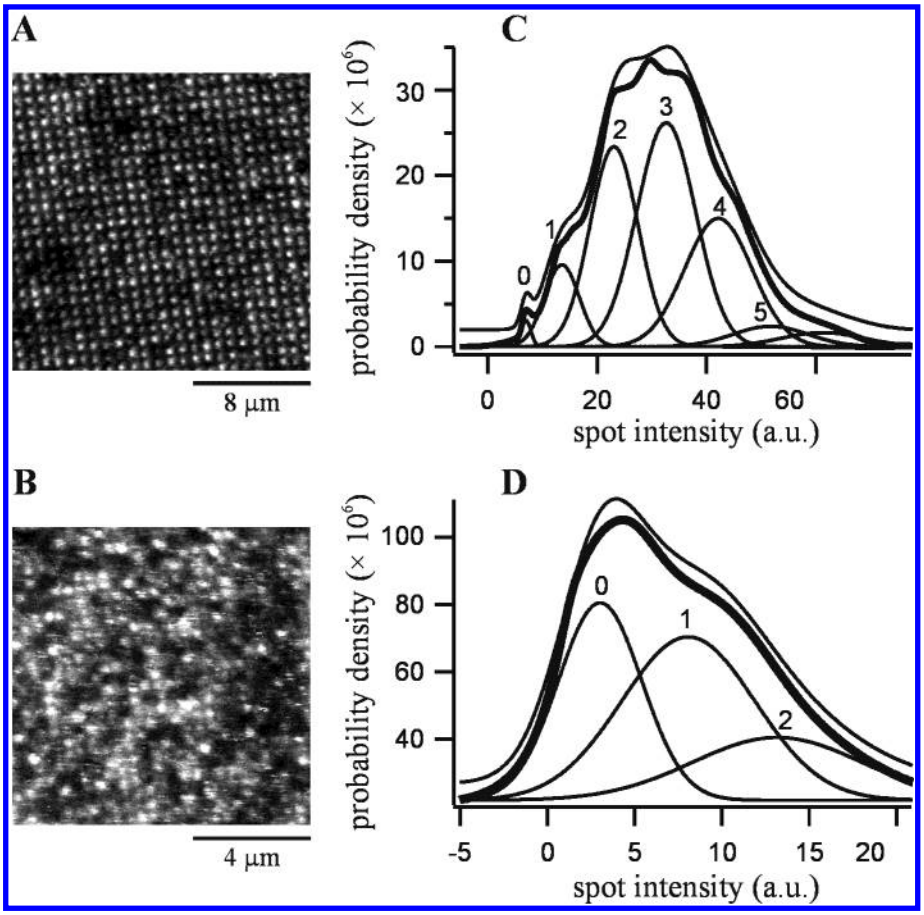

Figure 5. Scanning confocal fluorescence images of arrays of FITC-labeled antibodies that were microcontact printed on a glass substrate. These arrays were prepared by inking a high-resolution stamp with a 5 μg mL^{-1} solution of anti-goat antibody in PBS for 45 min. The antibodies were printed using (A) linelets or (B) 100-nm posts separated by 400 nm. (C and D) Distribution of the intensity of the fluorescent spots visible in the corresponding images. The thick lines correspond to the data, and the thinner lines (shifted slightly upward for better clarity) represent the fit of the data according to eq 4 and are composed of the underlying Gaussian curves. The numbers above the Gaussian curves correspond to the calculated numbers of protein for a given spot intensity.

the chromophores, the central position I_n and the width σ_{I_n} of the intensity distribution of an aggregate of n protein molecules can be calculated from the intensity I_B and width σ_{I_B} of the background and the intensity I_P and width σ_{I_P} of the contribution to the fluorescence due to one single protein molecule. σ_{I_P} is the standard deviation in the probability distribution of the intensity corresponding to a single protein molecule, which originates from the variable number of chromophores per protein and orientational effects. This standard deviation is independent of the number of proteins per spot.

$$I_n = I_B + nI_P \tag{6}$$

$$\sigma_{I_n}^2 = \sigma_{I_B}^2 + n\sigma_{I_P}^2 \tag{7}$$

By least-squares fitting the function $P(I)$, the probability P_n of finding n protein molecules per dot can be determined. In Figure 5D, the resulting fit to the data is displayed along with a decomposition into the Gaussian functions $G_n(I)$. The first three peaks, corresponding to $n = 0-2$ protein molecules per printed site, are clearly seen in the graph showing that a higher number of proteins does not lead to pronounced features in the curve in agreement between theory and experiment. This deconvolution can now be used to "count" the proteins at a given spot: given the fitted intensity I of an individual spot, for each number of proteins n the corresponding probability $P(n|I)$ is given as

$$P(n|I) = \frac{G_n(I)}{P(I)} \tag{8}$$

If the proteins adsorb from solution onto the dots on the stamp in an independent manner, the probability distribution of finding none or a few proteins per dots should follow a Poisson distribution. Indeed, the number of protein molecules per printed site measured by this method follows approximately a Poisson distribution. The mean number of protein molecules, printed from the 100 × 400 nm^2 linelets and from the 100-nm posts, is 3.5 and 1.1, respectively. This proportionality of the mean number of protein molecules for the larger and the smaller printed areas seems reasonable. For the smaller structures, a similar fraction (one-third) of unoccupied sites is inferred from the AFM and confocal fluorescence experiments, and sites with only one protein molecule are the most prevalent.

We selected a second type of protein to characterize μCP experiments on single protein molecules, using fluorescence. This protein is GFP; it is intrinsically fluorescent and has a comparatively large quantum yield of fluorescence.[37,53] Two types of experiments were conducted in which patterns of printed GFP molecules were characterized and photobleaching of single printed GFP molecules was observed. Contrary to the

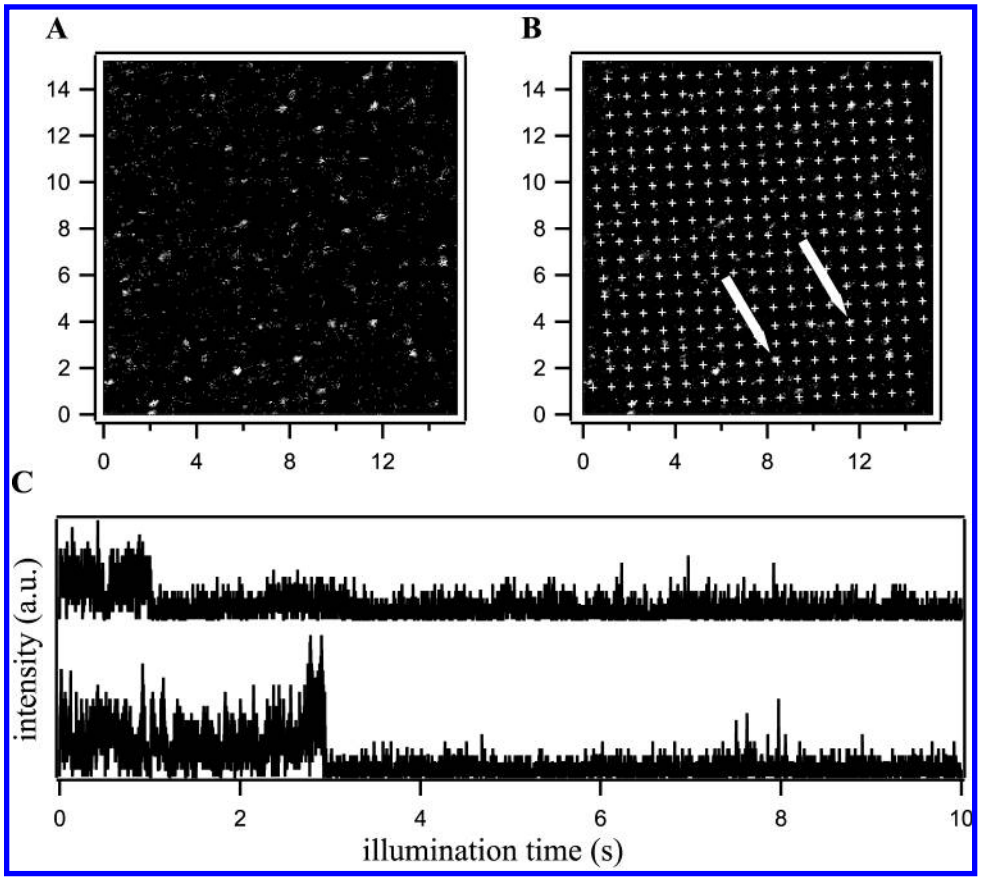

Figure 6. Scanning confocal fluorescence experiments of GFPs microcontact printed on glass using the linelets pattern of a stamp that was inked with a 50 μg mL^{-1} solution of GFP in PBS for 45 min. (A) The detected fluorescence does not reveal immediately the geometry of the printed pattern because some printed spots might be empty or occupied by denaturated, nonfluorescent GFPs. (B) Nevertheless, the observed fluorescent signals are sufficient to reconstruct the pattern statistically with a high degree of confidence. (C) In these analyses of the fluorescence as a function of time recorded at the position indicated by the arrows, the abrupt decrease in intensity corresponds to the bleaching of a single fluorophore. The lateral scales in (A) and (B) are in micrometers.

antibodies patterned in Figure 5, each GFP contains only one fluorescent center. Figure 6A shows a confocal fluorescence image of the linelet array. There is a small number of fluorescent protein molecules per lattice point, less than one on average. This is consistent with the less efficient inking observed for GFP, the possible denaturation or photobleaching of some of the GFPs, and the small size of the excitation beam ($<$250 nm) relative to the separation distance (800 nm) of the printed sites. For these reasons, low levels of fluorescence are detected on the surface, and the printed pattern is not directly recognizable. It is nevertheless possible to recompose the lattice, with a high degree of confidence, from a few regularly spaced fluorescent points. The matching observed and recomposed lattice points (Figure 6B) confirm that fluorescence originates from regularly spaced printed proteins. The attribution of the fluorescent points to single protein molecules is reinforced by the following photobleaching experiment. The position of the sample, with respect to the laser focus, was fixed at the two positions indicated in Figure 6B while recording the fluorescence signal, Figure 6C. One-step-photobleaching events are observed at both positions, revealing that one fluorescent GFP molecule only was printed at each site.

Discussion

Inking and Printing. Our experiments tend to show that microcontact printing of proteins at the 100-nm scale works in a way similar to that for larger scales. As observed previously, the transfer of the proteins from the stamp to the substrate is absolute in the area of contact,[18] at least when the substrate is hydrophilic glass.[23] The borders of the printed patterns are very sharp, even for assemblies comprised of only a few protein molecules (Figure 3, parts A and B), the overall number of defects is very low, and the printed patterns have an excellent contrast. This suggests that microcontact printing is a method of choice for creating high-resolution patterns of proteins on surfaces in which precise placement and low levels of defects are advantageous.[54] 100 nm represents an optimum in terms of lengthscale when using "semisoft" stamps; lower feature-sizes may require harder stamps, which may lead to a different mechanism of transfer of the proteins. The number of "defects", e.g., having too many or not enough proteins per printed site becomes high, especially for patterns of dots. Lowering the chance of covering a site of a pattern by inking a stamp with diluted solutions of proteins relaxes the need for having a pattern with dimensions similar to that of a protein molecule. The results in Figures 4−6 were achieved using patterns with a dimension larger than the maximal dimension of an antibody molecule. In principle, diluting the ink more to use patterns several hundreds of nanometers wide is possible, but keeping the placement of the printed proteins accurate helps to localize and characterize the patterns. At such a small scale, it is difficult to know how both the inking and printing conditions affect the printed patterns. The softness of stamps and the presence of proteins inked in the recessed regions of the pattern make it difficult to characterize an inked stamp using AFM or fluorescence microscopy, respectively. The characterization of a stamp after

inking and printing is consequently indirect. It is similarly difficult to predict accurately and to model possible deformations or rounding of high-resolution patterns during printing. The round shape of the posts might enhance the resolution of the printed patterns by reducing the effective contact area between the stamp and the substrate. We observed that proteins printed using the 100-nm posts were distributed within ±50 nm of the theoretical center of the dots. Stamps inked with proteins are employed in an apparently dry state, and previous experiments showed that lines of printed proteins can be very regular and straight. This suggests first that high-resolution patterns are not unstable to the extent of misplacing proteins during the printing step and, second, that proteins do not migrate during or after printing but form a "high-resolution ink." Together, these observations suggest that proteins adsorb randomly onto the dots of the stamps and transfer accurately to the surface during printing.

Microcontact printing proteins at high-resolution using continuous structures reveals an interesting phenomenon. Despite the same inking and printing conditions, the transfer of proteins from 100-nm-wide and from 40-nm-wide structures seems different, see Figure 3. The protein coverage of the glass substrate after printing, using the 40-nm-wide lines in Figure 3D, is less than 50%, whereas a complete and compact monolayer of antibodies (measured using fluorescence microscopy) forms on a planar PDMS surface inked under similar conditions. Previous studies on the influence of substrate topography on protein adsorption suggest that rougher surfaces prevent the aggregation of proteins more by lowering the lateral mobility of proteins during the adsorption process.[55,56] Another possibility is the interference of structures from the stamp on the lateral interactions that proteins in a dense layer can have with neighbors.[48,57] These possibilities may help to obtain isolated protein molecules on the stamp after the inking or printing steps. For the single protein patterning experiments, we expected the number of protein molecules per dot to be consequently sensitive to the concentration of the ink. Decreasing the concentration of the protein solution greatly increases the fraction of sites nonoccupied by proteins: ~60% of all potential printed sites are empty when using a concentration of antibodies in PBS $<1\ \mu g\ mL^{-1}$. Increasing the concentration induces the formation of aggregates, see Figure 4C. Above an inking concentration of $50\ \mu g\ mL^{-1}$, all sites of the pattern formed by the 100-nm posts are occupied by protein molecules arranged in a way similar to that of a dense layer formed when using larger structures. This underlines that the concentration of antibodies in the inking solution probably acts as a nonlinear parameter and becomes dominant for the microcontact printing of single protein molecules.

Concluding Remarks

A complete understanding of a specific process requires the independent observation of many single-molecule events. Ideally, this should allow for a deconvolution of the bulk behavior into all possible processes on the single molecule scale, weighted with the appropriate average. Observations of individual molecules have been proven to allow otherwise inaccessible insight into biochemical reactions and dynamics. Fluorescence techniques are prominent in these single-molecule studies. Scanning confocal fluorescence microscopy and related optical methods are easy to apply with little interference from the system under investigation. Such fluorescence studies are usually conducted by decreasing the observation volume and by diluting the species to be observed.[51,58] Analysis of single molecule fluorescence experiments is often hampered however, because the position of the isolated molecules is unknown. For example, the fluorescence detection of single-molecule binding events at interfaces could drastically improve the sensitivity of assays,[59] but it is necessary to localize precisely both binding partners to perform such assays. Several solutions based on co-localization assays were developed for this reason.[60] As an alternative, we propose the use of high-resolution μCP as a way to place single biomolecules on a nontreated planar surface reproducibly and rapidly and to observe them efficiently while minimizing nonspecific deposition or recognition events. Experiments based on AFM and confocal fluorescence microscopy point toward the successful printing of single antibody or GFP molecules. From the AFM measurements, protein molecules are localized within ±50 nm of their theoretical positions. As the uncertainty on the position of the protein is largely less than the lateral resolution achievable by confocal microscopy, all printing sites of a high-resolution pattern can be individually resolved. It is possible to improve the information retrieved from experiments using statistical algorithms and by filtering experimental data.[61] The density of information present in these high-resolution patterns is high because of the redundancy of the printed sites without the need to dilute the initial solutions of proteins. Therefore, the combination of μCP and of confocal fluorescence studies allows manipulation and characterization of molecular objects at the same time, which can usually only be done using local probing techniques. Microcontact printing at the single molecular level as it is achieved here benefits from the absence of noticeable diffusion of the protein molecules on the targeted substrate during printing and increases the chance of depositing only one protein molecule on some posts of the stamp during inking. Stamps made from harder elastomers could allow molding of smaller structures and improving the placement of single proteins. We think that the work presented here provides a better method to study single protein molecules on surfaces and, possibly, to construct artificial molecular structures by employing single molecules as high-resolution building blocks.

Acknowledgment. This work was partially supported by the Swiss National Science Foundation NFP 36 (Grant 31.55308.98). We thank S. Amontov, D. Juncker, H. Schmid, H. Wolf, and M. Wolf for discussions and P. F Seidler for his continuous support.

References and Notes

(1) *Molecular Electronics Devices*; Carter, F. L., Siatkowski, R. E., Wohltjen, H., Eds.; North-Holland: Amsterdam, 1986.

(2) Balzani, V.; Gomez-Lopez, M.; Stoddart, J. F. *Acc. Chem. Res.* **1998**, *31*, 405−414.

(3) Lindsey, J. S. *New J. Chem.* **1991**, *15*, 153−180.

(4) *Nanotechnology Towards a Molecular Construction Kit*; Ten Wolde, A., Ed.; STT Netherlands Study Centre for Technology Trends: The Hague, 1998.

(5) Ringsdorf, H.; Schlarb, B.; Venzmer, J. *Angew. Chem., Int. Ed. Engl.* **1988**, *27*, 113−158.

(6) Cornell, B. A.; Braach-Maksvytis, V. L. B.; King, L. G.; Osman, P. D. J.; Raguse, B.; Wieczorek, L.; Pace, R. J. *Nature* **1997**, *387*, 580−583.

(7) Granja, J. R.; Ghadiri, M. R. *J. Am. Chem. Soc.* **1994**, *116*, 10785−10786.

(8) Storhoff, J. J.; Mirkin, C. A. *Chem. Rev.* **1999**, *99*, 1849−1862.

(9) Fendler, J. H. *Chem. Mater.* **2001**, *13*, 3196−3210.

(10) Mehta, A. D.; Rief, M.; Spudich, J. A.; Smith, D. A.; Simmons, R. M. *Science* **1999**, *283*, 1689−1695.

(11) Florin, E.-L.; Rief, M.; Lehmann, H.; Ludwig, M.; Dornmair, C.; Moy, V. T.; Gaub, H. E. *Biosens. Bioelectron.* **1995**, *10*, 895−901.

(12) Kellermayer, M. S. Z.; Smith, S. B.; Granzier, H. L.; Bustamante, C. *Science* **1997**, *276*, 1112−1116.

(13) Rief, M.; Gautel, M.; Oesterhelt, F.; Fernandez, J. M.; Gaub, H. E. *Science* **1997**, *275*, 1295−1297.
(14) Browning-Kelley, M. E.; Wadu-Mesthrige, K.; Hari, V.; Liu, G.-Y. *Langmuir* **1997**, *13* 343−350.
(15) Strigl, M.; Simson, D. A.; Kacher, K.; Merkel, R. *Langmuir* **1999**, *15*, 7316−7324.
(16) Lee, K.-B.; Park, S.-J.; Mirkin, C. A.; Smith, J. C.; Mrksich, M. *Science* **2002**, *295*, 1702−1705.
(17) Dong, Y.; Shannon, C. *Anal. Chem.* **2000**, *72*, 2371−2376.
(18) Bernard, A.; Delamarche, E.; Schmid, H.; Michel, B.; Bosshard, H. R.; Biebuyck, H. A. *Langmuir* **1998**, *14*, 2225−2229.
(19) James, C. D.; Davis, R. C.; Kam, L.; Craighead, H. G.; Isaacson, M.; Turner, J. N.; Shain, W. *Langmuir* **1998**, *14*, 741−744.
(20) Martin, B. D.; Gaber, B. P.; Patterson, C. H.; Turner, D. C. *Langmuir* **1998**, *14*, 3971−3975.
(21) Bernard, A.; Renault, J.-P.; Michel, B.; Bosshard, H. R.; Delamarche, E. *Adv. Mater.* **2000**, *12*, 1067−1070.
(22) Lin, S. C.; Tseng, F. G.; Huang, H. M.; Huang, C. Y.; Chieng, C. C. *Fresenius J. Anal. Chem.* **2001**, *371*, 202−208.
(23) Tan, J. L.; Tien, J.; Chen, C. S. *Langmuir* **2002**, *18*, 519−523.
(24) Bernard, A.; Fitzli, D.; Sonderegger, P.; Delamarche, E.; Michel, B.; Bosshard, H. R.; Biebuyck, H. A. *Nature Biotechnol.* **2001**, *19*, 866−869.
(25) Renault, J. P.; Bernard, A.; Juncker, D.; Michel, B.; Bosshard, H. R.; Delamarche, E. *Angew. Chem., Int. Ed.* **2002**, *41*, 2320−2323.
(26) Lopez, G. P.; Biebuyck, H. A.; Härter, R.; Kumar, A.; Whitesides, G. M. *J. Am. Chem. Soc.* **1993**, *115*, 10774−10781.
(27) Singhvi, R.; Kumar, A.; Lopez, G. P.; Stephanopoulos, G. N.; Wang, D. I. C.; Whitesides, G. M.; Ingber, D. E. *Science* **1994**, *264*, 696−698.
(28) Kane, R. S.; Takayama, S.; Ostuni, E.; Ingber, D. E.; Whitesides, G. M. *Biomaterials* **1999**, *20*, 2363−2376.
(29) Yang, Z.; Chilkoti, A. *Adv. Mater.* **2000**, *12*, 413−417.
(30) Yang, Z.; Belu, A. M.; Liebmann-Vinson, A.; Sugg, H.; Chilkoti, A. *Langmuir* **2000**, *16*, 7482−7492.
(31) Inglis, W.; Sanders, G. H. W.; Williams, P. M.; Davies, M. C.; Roberts, C. J.; Tendler, S. J. B. *Langmuir* **2001**, *17*, 7402−7405.
(32) Kumar, A.; Whitesides, G. M. *Appl. Phys. Lett.* **1993**, *63*, 2002−2004.
(33) Xia, Y.; Whitesides, G. M. *Angew. Chem., Int. Ed. Engl.* **1998**, *37*, 550−575.
(34) Delamarche, E.; Schmid, H.; Bietsch, A.; Larsen, N. B.; Rothuizen, H.; Michel, B.; Biebuyck, H. A. *J. Phys. Chem. B* **1998**, *102*, 3324−3334.
(35) Schmid, H.; Michel, B. *Macromolecules* **2000**, *33*, 3042−3049.
(36) Michel, B.; Bernard, A.; Bietsch, A.; Delamarche, E.; Geissler, M.; Juncker, D.; Kind, H.; Renault, J. P.; Rothuizen, H.; Schmid, H.; Schmidt-Winkel, P.; Stutz, R.; Wolf, H. *IBM J. Res. Dev.* **2001**, *45*, 697−719.
(37) Tsien, R. Y. *Annu. Rev. Biochem.* **1998**, *67*, 509−544.
(38) Bietsch, A.; Michel, B. *J. Appl. Phys.* **2000**, *88*, 4310−4318.
(39) Delamarche, E.; Biebuyck, H. A.; Schmid, H.; Michel, B. *Adv. Mater.* **1997**, *9*, 741−746.
(40) Hui, C. Y.; Jagota, A.; Lin, Y. Y.; Kramer, E. J. *Langmuir* **2002**, *18*, 1394−1407.
(41) Prummer, M.; Hübner, C. G.; Sick, B.; Hecht, B.; Renn, A.; Wild, U. P. *Anal. Chem.* **2000**, *72*, 443−447.
(42) Chaudhury, M. K.; Whitesides, G. M. *Langmuir* **1991**, *7*, 1013−1025.
(43) Malotky, D. L.; Chaudhury, M. K. *Langmuir* **2001**, *17*, 7823−7829.
(44) Droz, E.; Taborelli, M.; Descouts, P.; Wells, T. N. C.; Werlen, R. C. *J. Vac. Sci. Technol. B* **1996**, *14*, 1422−1426.
(45) Silverton, E. W.; Navia, M. A.; Davies, D. R. *Proc. Natl. Acad. Sci. U.S.A.* **1977**, *74*, 5140−5144.
(46) Skaife, J. J.; Abbott, N. L. *Langmuir* **2000**, *16*, 3529−3536.
(47) Delamarche, E.; Bernard, A.; Schmid, H.; Bietsch, A.; Michel, B.; Biebuyck, H. A. *J. Am. Chem. Soc.* **1998**, *120*, 500−508.
(48) Petkov, J. T.; Gurkov, T. D.; Campbell, B. E. *Langmuir* **2001**, *17*, 4556−4563.
(49) Green, J.-B. D.; Novoradovsky, A.; Lee, G. U. *Langmuir* **1999**, *15*, 238−243.
(50) Fang, F.; Szleifer, I. *Biophys J.* **2001**, *80*, 2568−2589.
(51) *Single-Molecule Optical Detection, Imaging and Spectroscopy*; Basche, T., Moerner, W. E., Orrit, M., Wild, U. P., Eds.; VCH Verlag: Weinheim, Germany, 1997.
(52) Schmidt, T.; Schütz, G. J.; Gruber, H. J.; Schindler, H. *Anal. Chem.* **1996**, *68*, 8, 4397−4401.
(53) Peterman, E. J. G.; Brasselet, S.; Moerner, W. E. *J. Phys. Chem. A* **1999**, *103*, 10553−10560.
(54) Lu, H. B.; Homola, J.; Campbell, C. T.; Nenninger, G. G.; Yee, S. S.; Ratner, B. D. *Sens. Actuators B* **2001**, *74*, 91−99.
(55) Ramsden, J. J.; Bachmanova, G. I.; Archakov, A. I. *Phys. Rev. E* **1994**, *50*, 5072−5076.
(56) Calonder, C.; Tie, Y.; Van Tassel, P. R. *Proc. Natl. Acad. Sci. U.S.A.* **2001**, *98*, 10664−10669.
(57) Petkov, J. T.; Gurkov, T. D.; Campbell, B. E.; Borwankar, R. P. *Langmuir* **2000**, *16*, 3703−3711.
(58) Kolodny, L. A.; Willard, D. M.; Carillo, L. L.; Nelson, M. W.; Van Orden, A. *Anal. Chem.* **2001**, *73*, 1959−1966.
(59) Löscher, F.; Böhme, S.; Martin, J.; Seeger, S. *Anal. Chem.* **1998**, *70*, 3202−3205.
(60) Trabesinger, W.; Hecht, B.; Wild, U. P.; Schütz, G. J.; Schindler, H.; Schmidt, Th. *Anal. Chem.* **2001**, *73*, 1100−1105.
(61) Ratcliff, G. C.; Erie, D. A. *J. Am. Chem. Soc.* **2001**, *123*, 5632−5635.